

Particle-in-cell modeling of the nanosecond field emission driven discharge in pressurized hydrogen

Dmitry Levko,¹ Shurik Yatom,² and Yakov E. Krasik³

¹Department of Aerospace Engineering and Engineering Mechanics, The University of Texas at Austin, Austin, Texas 78712, USA

²Princeton Plasma Physics Laboratory, Princeton, New Jersey 08543, USA

³Department of Physics, Technion, 32000 Haifa, Israel

(Received 1 January 2018; accepted 11 February 2018; published online 27 February 2018)

The high-voltage field-emission driven nanosecond discharge in pressurized hydrogen is studied using the one-dimensional Particle-in-Cell Monte Carlo collision model. It is obtained that the main part of the field-emitted electrons becomes runaway in the thin cathode sheath. These runaway electrons propagate the entire cathode-anode gap, creating rather dense ($\sim 10^{12} \text{ cm}^{-3}$) seeding plasma electrons. In addition, these electrons initiate a streamer propagating through this background plasma with a speed $\sim 30\%$ of the speed of light. Such a high streamer speed allows the self-acceleration mechanism of runaway electrons present between the streamer head and the anode to be realized. As a consequence, the energy of runaway electrons exceeds the cathode-anode gap voltage. In addition, the influence of the field emission switching-off time is analyzed. It is obtained that this time significantly influences the discharge dynamics. *Published by AIP Publishing.*

<https://doi.org/10.1063/1.5021129>

I. INTRODUCTION

The research of high-voltage (HV) nanosecond (ns) pulse discharges in pressurized gases has attracted considerable attention since the 1960s^{1–4} because of the interesting phenomena involved and their important applications, such as plasma assisted ignition and combustion, pulsed gaseous lasers, and the generation of electron beams and x-rays.⁴

Depending on the voltage applied, different physical phenomena are involved and govern this type of pulse discharge.^{1–4} At very high voltages ($>100 \text{ kV}$), the electric field at the cathode surface, having micro-protrusions, reaches $\sim 10^9 \text{ V/m}$, which is sufficient for intense electron field emission (FE). Numerous experimental and numerical modeling studies^{5–21} have shown that at such an extremely high electric field, one can obtain runaway electrons (RAEs), i.e., electrons that acquire more energy during their acceleration by an electric field along a mean free path than they lose in inelastic collisions with neutrals or ions. RAEs propagate the entire cathode-anode (CA) gap, experiencing only a few collisions and generating a seeding (secondary) electron background. This seed allows the bridging of the CA gap by dense plasma on the sub-ns timescale, which is impossible without RAEs.

In order to obtain RAE generation, one needs to apply an electric field exceeding the threshold value E_{cr} , which depends on the background gas type and its pressure.^{1–4} At normal atmospheric pressure, for many gases, this electric field varies in the range of $1\text{--}5 \times 10^7 \text{ V/m}$. Thus, in the case where the electric field at the cathode surface is $\sim 10^9 \text{ V/m}$, the main part of FE electrons becomes RAEs, obtaining energy $\gg 10 \text{ keV}$ in the vicinity of the cathode.¹⁷ However, depending on the anode and cathode electrode geometry, CA gap, and the pressure and type of the gas, these electrons do not necessarily continue to be RAEs during their propagation

toward the anode. Only if the electric field is $>E_{cr}$, do high-energy electrons continue to accelerate, i.e., remain RAEs. However, if the electric field in the CA gap is significantly smaller than E_{cr} , a significant part of these high-energy electrons' energy can be dissipated during their propagation toward the anode through elastic and inelastic collisions.⁵

HV discharge in an air-filled diode at atmospheric and elevated pressures in a non-uniform electric field in a ns-timescale has been studied in many laboratories worldwide.^{1–16,20,21} For instance, the results reported in Ref. 16 showed that the beginning of the electron generation precedes the appearance of light emission at the blade-type cathode edge, indicating that RAE generation occurs via FE prior to the formation of the cathode explosive plasma. Furthermore, it was found that the measured RAE energy spectrum shows that the maximal energy of electrons arriving at the anode is $\leq e\varphi_{CA}$, where e is the electron charge and $\varphi_{CA} \approx 120 \text{ kV}$ is the applied voltage, and this spectrum can be fitted with Maxwell distribution for electrons with energies $\geq 20 \text{ keV}$. The discharge has the form of separate plasma channels, originating at the cathode edge, and the light emission front propagates toward the anode at a velocity of $\sim 10^9 \text{ cm/s}$, corresponding to the velocity of electrons with an energy of $\sim 300 \text{ eV}$, i.e., with sufficient energy to allow ionization and excitation processes. This propagation velocity decreases with an increase in the gas pressure and the CA gap length. At atmospheric gas pressure, these plasma channels take the form of diffusive jets, and this form is changed to that of contracted channels as the pressure increases to $\geq 2 \times 10^5 \text{ Pa}$.

An interesting observation about the electrons with anomalously high energy was reported and discussed, for instance, in Refs. 1–4 and 22–24. These electrons are the electrons having energy that exceeds the value $e\varphi_{max}$, where

φ_{max} is the maximum amplitude of the voltage pulse applied to the cathode. The most probable explanation of this phenomenon is “anomalous” electron generation due to the self-acceleration mechanism, as suggested by Askaryan²⁵ (see Sec. IV).

The results presented in this paper continue those of the studies reported in Refs. 16 and 17. In the present study, the self-consistent one-dimensional Particle-in-Cell Monte Carlo collision (1D PIC/MCC) model was used with more accurate treatment of FE electrons. This treatment allows us to obtain the results that were only speculated in earlier research. It should also be noted that we focused only on the streamer discharges, the time- and space evolution of which is governed by FE electrons opposite to the streamers propagating through the natural electron background, which was analyzed in recently published review papers (see Refs. 26–28 and references therein).

II. NUMERICAL MODEL

In order to study HV high-pressure discharge, we updated the model developed in Ref. 17. This is a 1D PIC/MCC model in cylindrical coordinates considering a coaxial diode. The cathode is the inner rod made of copper with radius $r_C \sim 3 \mu\text{m}$, and the anode is the outer cylinder having radius $r_A = 1 \text{ cm}$. The anode is grounded, while the cathode voltage is changed in time as $U_C = U_0 \cdot \sin(2\pi t/T)$, where $U_0 = -100 \text{ kV}$ and $T = 10 \text{ ns}$, i.e., the voltage rise time is $T/4 = 2.5 \text{ ns}$. This voltage temporal dependence was used to fit the voltage waveforms obtained in experimental research¹⁶ [see Fig. 3(g) in Ref. 16]. The diode is filled with molecular hydrogen (H_2) at a pressure of $P = 2 \times 10^5 \text{ Pa}$ and a temperature of $T_g = 300 \text{ K}$.

The model accounts for the electron-neutral momentum transfer collisions, excitation of the first three electronic levels of H_2 , and excitation of rotational and vibrational levels, dissociation, and ionization (see Fig. 1). If ionization occurs, one electron-ion (H_2^+) pair is added to the simulation domain. Note that excitation and dissociation collisions do not lead to the generation of new species. These collisions lead only to the electron energy losses that must be considered for the accurate treatment of the total electron energy losses. For electron- H_2 ionization cross sections, the NIST

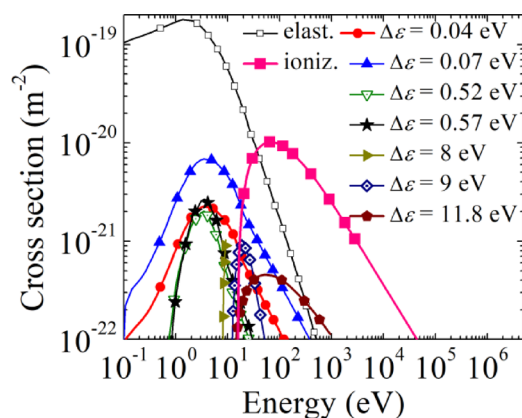


FIG. 1. Electron- H_2 cross sections used in the 1D PIC/MCC model.

database was used.²⁹ The cross sections of other collisions were taken from Biagi’s database.³⁰ The collisions between electrons and the possible products of dissociation of H_2 (e.g., H) were not considered in the present model.

In the model, the electron FE from the cathode is considered using the Fowler-Nordheim (FN) equation³¹

$$j_{FN} = 6.2 \times 10^{-6} \frac{(\varepsilon_F/\varphi)^{1/2} (E)^2}{\varepsilon_F + \varphi} \cdot \exp \left[-\frac{6.85 \times 10^7 \varphi^{3/2} \xi}{E} \right]. \quad (1)$$

Here, $\varepsilon_F = 7.0 \text{ eV}$ is the Fermi energy, E is the electric field at the cathode surface, and $\varphi = 4.4 \text{ eV}$ is the work function for the cathode made of copper.³¹ ξ is the correction factor, which depends on both E and φ .³¹

In the model considered here, the cathode material is taken into account only through the work function φ . For many materials, the work function varies in the range of $\sim 2\text{--}5 \text{ eV}$ ³² which can significantly influence the discharge dynamics (see, for instance, discussion in Refs. 33 and 34). Namely, the decrease in the cathode material work function will decrease the time when the noticeable FE is obtained (see discussion in Sec. III). This, in turn, will influence the energy of RAEs and can change the discharge dynamics.

The exponential dependence of the FE current on the electric field [Eq. (1)] renders the modeling of high-pressure discharges driven by FE very challenging. Indeed, the discharge, ignited by a small FE current, very quickly transfers to a dense plasma generated in the CA gap, and a thin non-neutral sheath is formed between the plasma boundary and the cathode surface. The potential drop on this sheath, depending on the plasma resistivity, can reach a significant part of the voltage applied to the CA gap. The latter leads to an increase in a few orders of magnitude in the FE current due to the increase in the electric field at the cathode surface. For instance, in the conditions of this study, the FE current density varies in the range of $10^6\text{--}10^{10} \text{ A/m}^2$. This temporal and spatial evolution of the FE process, plasma, and sheath formation is accompanied by a variation in the plasma density in the range of $10^9\text{--}10^{23} \text{ m}^{-3}$. To cover such a wide range of densities with the constant weight of “macro”-particles (i.e., the number of real particles in each computational particle), one needs to use $\sim 10^9$ “macro”-particles even in 1D simulation. In order to overcome this computational restriction, we implemented an algorithm for merging “macro”-particles (for details, see Ref. 35) to keep the overall “macro”-particle number below a specified threshold. In this study, this threshold was set at 10^6 for each species. By this method, two “macro”-particles of the same type neighboring in the phase space are merged. The velocity and position of the new “macro”-particle are defined as the average values of the velocities and positions of the two merged particles.

However, this merging algorithm is not effective for energetic electrons generated as a part of the FE electrons because the number of these energetic electrons is significantly smaller than that of the secondary electrons generated in the CA gap. These energetic electrons belong to the tail of the electron energy distribution function, and the velocity of

their neighbors in phase space can be considerably smaller. Hence, the merging of energetic and “cold” plasma electrons, the energy of which is only a few tens of eV, leads to the numerical “cooling” of the former. To overcome this artificial cooling, FE and plasma electrons were considered as two different types of “macro”-particles. Note that the plasma electrons are all electrons generated in the gap due to the gas ionization.

To facilitate the model’s implementation, FE electrons were not divided into fast and slow groups because, as shown in the following, all FE electrons finally become RAEs. The weight of FE electrons w_{FE} was kept constant during the simulation, i.e., the merging algorithm was not applied to these particles. Namely, the weight of FE “macro”-particles was selected to keep their total number below the set threshold value of 10^6 . The weight of plasma electron macro-particles w_p was varied in time, i.e., they were merged during the simulation. For brevity, hereinafter, FE and plasma electrons are considered to represent the corresponding “macro”-particles. The collisions for both groups of electrons were modeled using the same Monte Carlo algorithm. If the electron (FE or plasma) produces ionizing collisions with the H_2 molecules, a new electron/ion pair was added to the simulation domain. Because of the difference in weights for the FE and plasma electrons, an additional source term $S_i(x)$ was introduced. This source accounts for the ionization events produced only by the FE electrons. If the FE electron experiences an ionizing collision, one electron with the weight w_{FE} is added to $S_i(x)$. In each time step, the function $S_i(x)$ was checked, and if the condition $S_i(x)/w_p \geq 1$ was satisfied, the number $\text{int}(S_i(x)/w_p)$ of electrons was added to the plasma electrons. The space step used in this model is $\Delta x = 0.2 \mu\text{m}$, allowing the resolution of the parameters of the spatial gradients inside the CA, including the cathode sheath. The time step, $\Delta t = 10^{-15}$ s, is dictated by the Courant condition.

III. RESULTS AND DISCUSSION

A. Discharge dynamics

This subsection presents the results of the 1D PIC/MCC simulations obtained for H_2 gas at pressure $P = 2 \times 10^5$ Pa. For a cathode radius of $3 \mu\text{m}$, the FE current reaches the value of $\sim 10^6$ A/m² at $t \approx 1.3$ ns, which leads to the emission of the first “macro”-particles to the CA gap. At this time, the applied voltage reaches 73 kV, and the electric field at the cathode surface is $E_C \approx 2.8 \times 10^9$ V/m (see Fig. 2). This electric field significantly exceeds $E_{cr} \sim 6 \times 10^7$ V/m necessary for the electrons to run away in H_2 gas at $P = 2 \times 10^5$ Pa. The latter results in FE electrons becoming runaway almost immediately after their injection into the CA gap, acquiring energy > 1 keV at a distance of a few microns from the cathode. These energetic electrons also generate electron/ion pairs during their acceleration toward the anode. The total electron-neutral collision cross section of 2-keV electrons in H_2 gas is $\sim 2 \times 10^{-21}$ m², resulting in the mean free path of these electrons in H_2 gas, $\lambda \sim 10 \mu\text{m}$. One can see that, at $r = 13 \mu\text{m}$, the electric field $E(r) = U_C / [r \cdot \ln(r_A/r_C)]$ decreases ~ 3.6 times, but its value is still

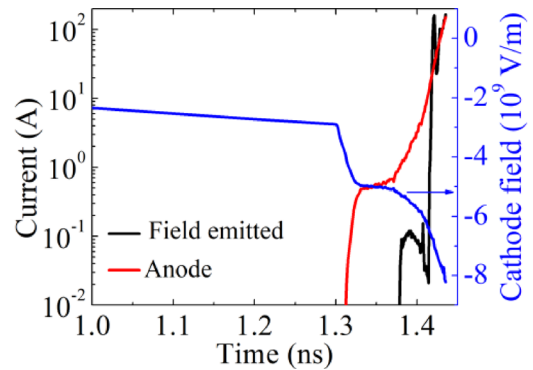


FIG. 2. Time evolution of the field emission current and electron current through the anode and the electric field at the cathode.

significantly larger than E_{cr} . Only at radii > 0.8 mm, does the electric field become smaller than E_{cr} . Hence, the plasma electrons generated in the vicinity of the cathode also become RAEs although the energy of these electrons is smaller than that of FE electrons.

The simulation results show that, in the CA gap, $\sim 99\%$ of the plasma charged particles is generated by the plasma electrons and only $\sim 1\%$ is generated by the FE electrons. This result is related to the significantly larger number density of plasma electrons, n_e , than that of FE electrons, n_{RAE} ($n_{RAE}/n_e \sim 0.01$), as well as to the fact that the ionization frequency ν_i of plasma electrons having energy $\varepsilon_e \ll 100$ eV is much larger than the ν_i of FE electrons with energy $\varepsilon_e \gg 1$ keV.

Figure 3 shows the space evolution of the electron density and potential at different times of the discharge development. Figure 3(a) shows that at $t \approx 1.3$ ns, the density of the plasma generated in the vicinity of the cathode reaches $n_e \sim 10^{14}$ cm⁻³. This plasma screens the applied electric field, leading to the formation of a thin (a few microns) cathode sheath [Fig. 3(c)]. This results in an increase in the electric field at the cathode surface and in a significant increase in the FE current (Fig. 2). The latter, in its turn, leads to a further increase in the plasma electron density. Figure 3(a) shows that at $t \approx 1.4$ ns, the plasma density reaches $n_e \sim 10^{16}$ cm⁻³ in the cathode vicinity. The sheath thickness obtained at this time is $l_{sh} \sim 20 \mu\text{m}$, and the sheath voltage is $U_{sh} \sim 25$ kV.

Figure 4(a) presents the energy phase space of emitted electrons at 1.36 ns. One can see that the FE electrons are accelerated in the sheath, acquiring energy up to $\sim eU_{sh}$, i.e., these electrons become RAEs. The electron- H_2 ionization cross section of 20-keV electrons is $\sigma_{ion} \sim 9 \times 10^{-23}$ m². The mean free path of these electrons is $\lambda \sim 100 \mu\text{m}$, and the ionization collision frequency is $\nu_{ion} \sim 3.6 \times 10^{11}$ s⁻¹. These 20-keV electrons propagate in the electric field $E \sim 10^7$ V/m. The energy gained by 20-keV electrons between two consecutive ionization collisions can be estimated as $\Delta\varepsilon = q_e^2 E^2 / (2m_e \nu_{ion}^2) \approx 66$ eV which significantly exceeds the ionization energy of an H_2 molecule (15.4 eV). Thus, the FE electrons that become runaway in the cathode sheath propagate the entire CA gap, remaining RAEs.

One can conclude from Fig. 3(a) that the FE-driven discharge can be described using the commonly accepted

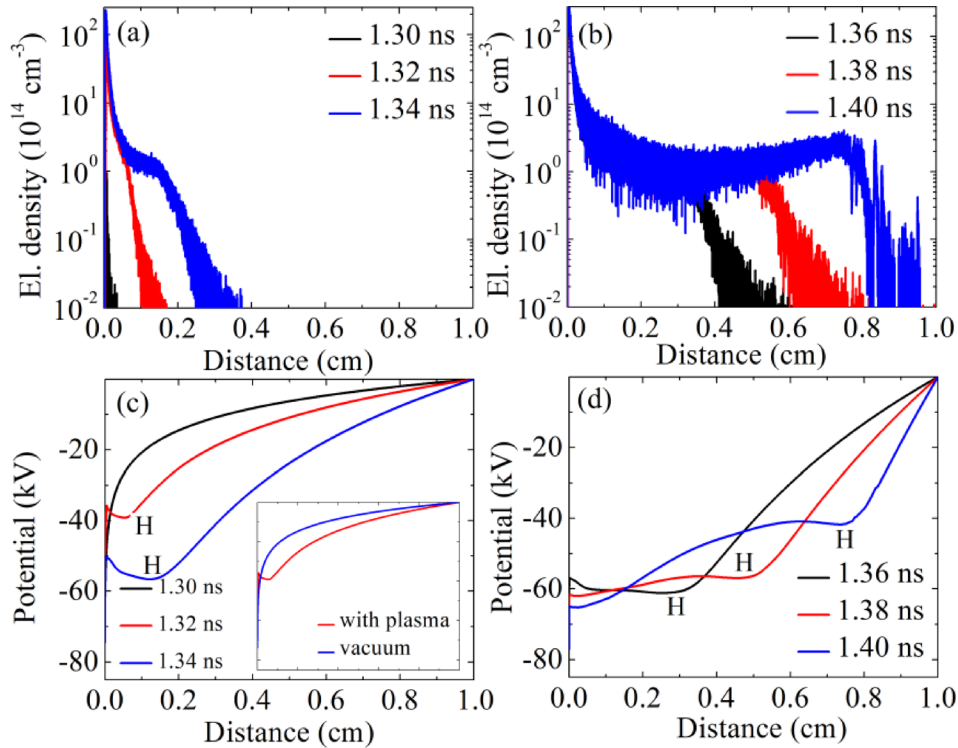


FIG. 3. [(a) and (b)] Electron density and [(c) and (d)] potential obtained at different times; $P = 2 \times 10^5$ Pa. The inset in (c) shows the potential distribution with and without plasma at $t = 1.32$ ns. H denotes the position of the streamer head.

model³¹ of the anode-directed streamer [see Figs. 3(b) and 3(d)]. Following Ref. 31, an anode-directed streamer is defined as a quasi-neutral plasma jet (density $\sim 10^{13} - 10^{15} \text{ cm}^{-3}$) acquiring a large part of the cathode potential and propagating toward the anode. A high-intensity electric field is obtained only at the streamer head, where the plasma quasi-neutrality is violated because of space separation between the fast electrons and ions at that location. At the beginning of FE, i.e., when the first FE electrons become accounted for in the simulations, a low-density ($< 10^{12} \text{ cm}^{-3}$) plasma is formed in the vicinity of the cathode, transforming very quickly to the propagating streamer. A large part of FE electrons becomes RAEs, experiencing very few ionization collisions during their propagation toward the anode. Nevertheless, these ionization collisions lead to the formation of seeded electrons in front of the streamer head (see Fig. 4) with a density of $\sim 10^{12} \text{ cm}^{-3}$, which significantly exceeds the natural background electron density ($\sim 10^3 \text{ cm}^{-3}$) commonly assumed in streamer models.³¹ This result, namely, the increasing streamer velocity for the increasing density of the seeding background, qualitatively agrees with the theory developed in Ref. 36.

A high electric field ($\sim 1 - 2 \times 10^7 \text{ V/m}$) is obtained at the streamer head, which we determined as points H in Figs. 3(c) and 3(d), where the maximal negative potential is realized. This electric field accelerates seeded electrons at those locations to energies exceeding the ionization threshold of H_2 , thus supporting the streamer propagation. Since the density of seeded electrons is $\sim 10^{12} \text{ cm}^{-3}$, the streamer obtained during the discharge supported by FE and by these seeded electrons, propagates significantly faster than that considered, for instance, in Ref. 31. One can see in Fig. 3 that the streamer propagates a distance of $\sim 0.8 \text{ cm}$ during 100 ps, resulting in a streamer average velocity $v_{fr} \sim 8 \times 10^7 \text{ m/s}$. Here, let us note that the average velocity of the conventional anode-directed streamer is only $\sim 10^5 \text{ m/s}$.³¹

Figure 4 shows the typical energy phase spaces of the plasma and FE electrons at $t = 1.36$ ns. One can see in Fig. 4(a) that part of the plasma electrons also becomes RAEs. These plasma electrons were generated in the cathode sheath due to the gas ionization by FE electrons. In addition, the electric field at point H [see Fig. 4(a)] is $\leq 2 \times 10^7 \text{ V/m}$, i.e., it is significantly smaller than the value of E_{cr} necessary for RAE generation in H_2 . Thus, the streamer head cannot be

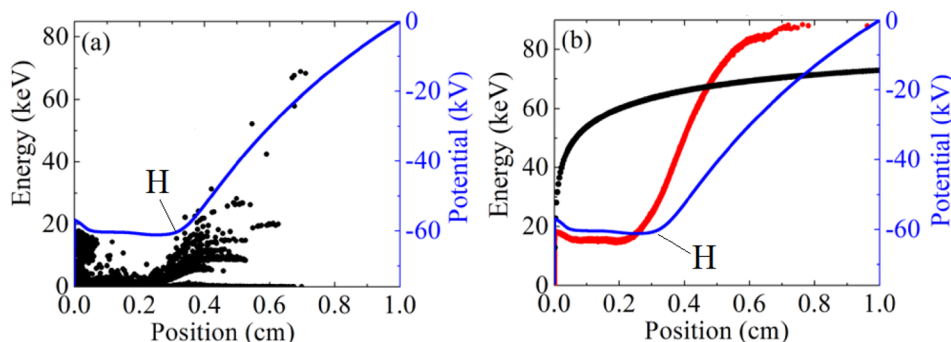


FIG. 4. (a) Energy phase space of plasma electrons and (b) phase space of field emission (FE) at $t = 1.36$ ns; $P = 2 \times 10^5$ Pa. The blue line shows the distribution of potential at the same time. Black dots in Fig. 3(b) show the energy phase space of FE electrons for vacuum conditions.

considered a source of RAE generation under the given conditions for H_2 gas.

In Fig. 4(b), one can see that the energy of FE electrons $\varepsilon_{e,em}$ reaches ~ 88 keV, while the cathode potential at $t = 1.36$ ns is only -75.4 kV, i.e., $\varepsilon_{e,em} > e|U_C|$. Let us note that the number of such “anomalous” electrons is $\sim 0.1\%$ of the total number of electrons obtained at that time in the CA gap. The anomalous high energy of FE electrons can be explained by the self-acceleration mechanism suggested by Askaryan.²⁵ The simulation results show that, because of the high density ($\sim 10^{12} \text{ cm}^{-3}$) of seed electrons generated by RAEs in front of the streamer head, one obtains streamer propagation toward the anode with $v_{fr} \sim 8 \times 10^7$ m/s and an electric field at the streamer head of $\sim 10^7$ V/m. In the frame of the fast propagating streamer, the RAEs present between the streamer head and the anode acquire additional energy (with respect to $e|U_C|$), which can reach tens of keV. Let us note that sometimes in the literature such a fast propagating streamer is called an ionization wave.

Figure 5 shows the electron density and potential distributions and the energy phase spaces of plasma and FE electrons obtained at $t = 1.42$ ns when the streamer bridges the CA gap. At that time, the cathode sheath width is $l_{sh} \sim 1.5 \mu\text{m}$ with a voltage drop of ~ 4.6 kV, and the plasma density in the vicinity of the cathode sheath reaches $\sim 10^{17} \text{ cm}^{-3}$. One can see that an electric field of $\sim 7 \times 10^6$ V/m is present in the plasma [see Fig. 5(a)], indicating the high resistivity of the plasma. A similar electric field value of $\sim 3 \times 10^6$ V/m in the plasma channel was recently measured in the HV ns-timescale discharge in H_2 gas at a pressure of 2×10^5 Pa.¹⁶

The energy phase space of FE electrons [Fig. 5(c)] shows that these electrons can be considered RAEs although their energy in the anode vicinity is smaller than $e|U_C|$ [$U_C = -77.9$ kV, Fig. 4(a)]. The energy of FE electrons entering the plasma bulk from the cathode sheath is only ~ 4.6 keV, but it is sufficient for these electrons to remain in the acceleration in the weaker electric field obtained in the plasma bulk ($\sim 7 \times 10^6$ V/m).

The energy phase space of plasma electrons shows the presence of two groups of energetic (up to several keV) electrons located close to the cathode and anode [see Fig. 5(b)]. Close to the anode are the electrons that became RAEs before the streamer bridged the CA gap, whereas close to the cathode are energetic electrons generated in the cathode sheath by FE electrons. The latter cannot be considered

RAEs despite the fact that these electrons enter the plasma bulk with an energy of ~ 2.5 keV. The latter is explained by the insignificant electric field in the plasma bulk, which is smaller than E_{cr} . Thus, almost all the energy of these energetic electrons is dissipated during their propagation toward the anode.

B. Role of the FE electrons in streamer propagation dynamics

In order to understand the role of FE electrons in the dynamics of streamer propagation and the distributions of the plasma density and potential in the CA gap, additional PIC/MCC simulations were performed. In these simulations, the FE was artificially switched off with a time delay τ with respect to the beginning of electron emission. It is understood that in the experimental conditions, FE will be transferred to explosive emission plasma formation. However, because of the fast (up to $\sim 5 \times 10^4$ m/s) expansion of the plasma acquiring cathode potential, the electric field at the plasma boundary decreases quickly below E_{cr} and the electrons emitted from the boundary of this plasma cannot be considered RAEs.

Figure 6 shows the electron density and potential distributions at different times with respect to $\tau = 1.33$ ns. At $t = 1.33$ ns [see Fig. 3(a)], the streamer propagates ~ 0.2 cm and the anode current reaches ~ 0.8 A (see Fig. 2). At that time, one obtains that between the dense ($> 10^{14} \text{ cm}^{-3}$) plasma [see point D in Figs. 6(a) and 6(c)] and anode, there is a plasma ($0.1 \text{ cm} < r < 0.3 \text{ cm}$) formed by the RAEs and plasma electrons prior to the FE switch-off with density $\leq 10^{13} \text{ cm}^{-3}$. Later in time, one obtains [see Fig. 6(b)] rather gradual plasma formation toward the anode. Indeed, a comparison of the distributions presented in Figs. 3 and 6 shows that after the FE switch-off, there is no fast propagation of the streamer as compared with the case of continuous FE of electrons. The latter is explained by the fact that the conditions necessary for self-consistent fast streamer propagation are not satisfied at $\tau = 1.33$ ns. Indeed, at this time, the electric field at the “head” of the streamer is $\sim 10^7$ V/m, i.e., it is smaller than the electric field necessary for the H_2 breakdown by means of the streamer. In addition, at this time, only a small number of RAEs cross the CA gap and therefore the density of the seeded electrons are not sufficient to obtain a fast propagating streamer.

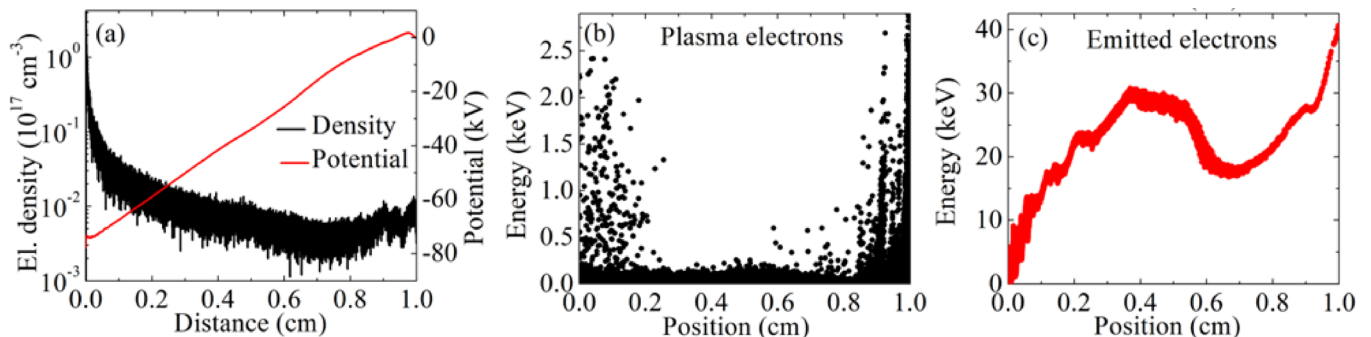


FIG. 5. (a) Electron density and potential, (b) phase space of plasma electrons, and (c) energy phase space of field emission electrons obtained at $t = 1.42$ ns.

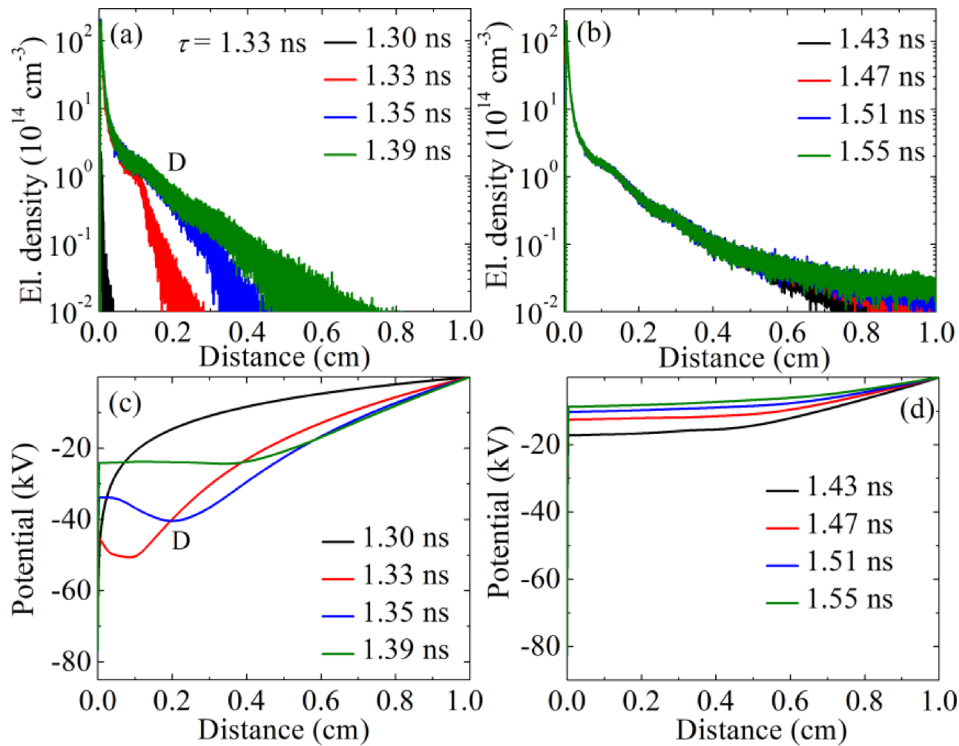


FIG. 6. [(a) and (b)] Electron density and [(c) and (d)] potential distributions obtained at different times; H_2 gas pressure is 2×10^5 Pa, and field emission is switched-off at $\tau = 1.33$ ns.

Figure 6(d) shows the potential distributions at $t > 1.43$ ns, when the CA gap is bridged by the plasma with density $> 10^{13} \text{ cm}^{-3}$. At these times, there are three regions with different plasma densities and potential distributions, namely, a thin cathode sheath ($l_{sh} \sim 30 \mu\text{m}$), where ions' acceleration toward the cathode occurs, the region of quasi-neutral plasma, where the electric field is $\sim 10^5$ V/m, and the anode layer with an electric field of $\sim 10^6$ V/m. The anode layer formation is dictated by the current continuity since the plasma density in the vicinity of the cathode sheath edge is $\sim 10^3$ times larger than that in the anode vicinity [see Fig. 6(b)].

The energy phase spaces of FE electrons prior to and after FE termination at $\tau = 1.33$ ns are shown in Fig. 7. One can see that the energy of FE electrons does not exceed $e|U_C|$, as was obtained with continuous electron FE. Moreover, at 0.14 ns after the FE is switched off, the energy of electrons reaching the anode already does not exceed 25%

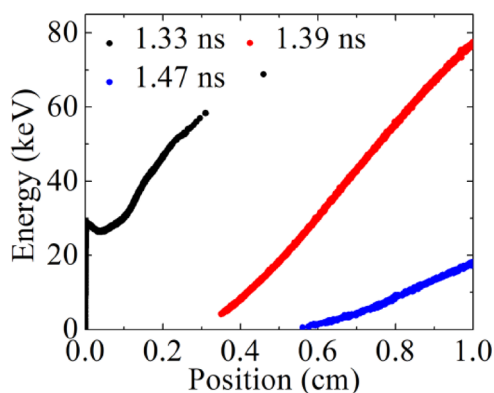


FIG. 7. Phase space of field emission (FE) electrons obtained at three different times; H_2 gas pressure is 2×10^5 Pa, and FE is switched off at $\tau = 1.33$ ns.

of $e|U_C|$. The latter is explained by the drastic decrease in the electric field in the CA gap [see Fig. 6(d)], resulting in that FE electrons cannot be now considered RAEs.

The simulation results for electron density and potential distributions obtained at different times for $\tau = 1.4$ ns are shown in Fig. 8. One can see that a 0.07 ns time delay in switch-off of the FE as compared with the previous case changes drastically the discharge dynamics; namely, one can clearly see the propagation of the fast streamer, similarly to the case of continuous electron FE.

Such a significant sensitivity to the value of τ formation and the fast propagation of the streamer is related to the number of FE electrons emitted prior to the switch-off instant. Indeed, the anode current reaches 2 A at $t = 1.4$ ns (see Fig. 2), which is 2.5 times larger than the anode current obtained at $t = 1.33$ ns. The latter is related to the significantly larger number of FE electrons injected into the CA gap prior to the FE switch-off for $\tau = 1.4$ ns than for $\tau = 1.33$ ns and the larger number of RAEs present in the CA and producing a larger density of seeded electrons across the entire CA gap (see Figs. 7 and 9). However, even at $\tau = 1.4$ ns, when one obtains fast streamer propagation after FE termination, the energy of FE reaching the anode does not exceed $e|U_C|$ because of the significantly smaller electric field at the streamer head.

IV. SUMMARY

High-voltage nanosecond discharge in hydrogen was studied using the one-dimensional Particle-in-Cell Monte Carlo collision model. The discharge was driven by the electron field emission from the small-curvature cathode.

It was obtained that the main part of FE electrons becomes runaway in the thin cathode sheath. These runaway electrons propagate the entire cathode-anode gap, creating

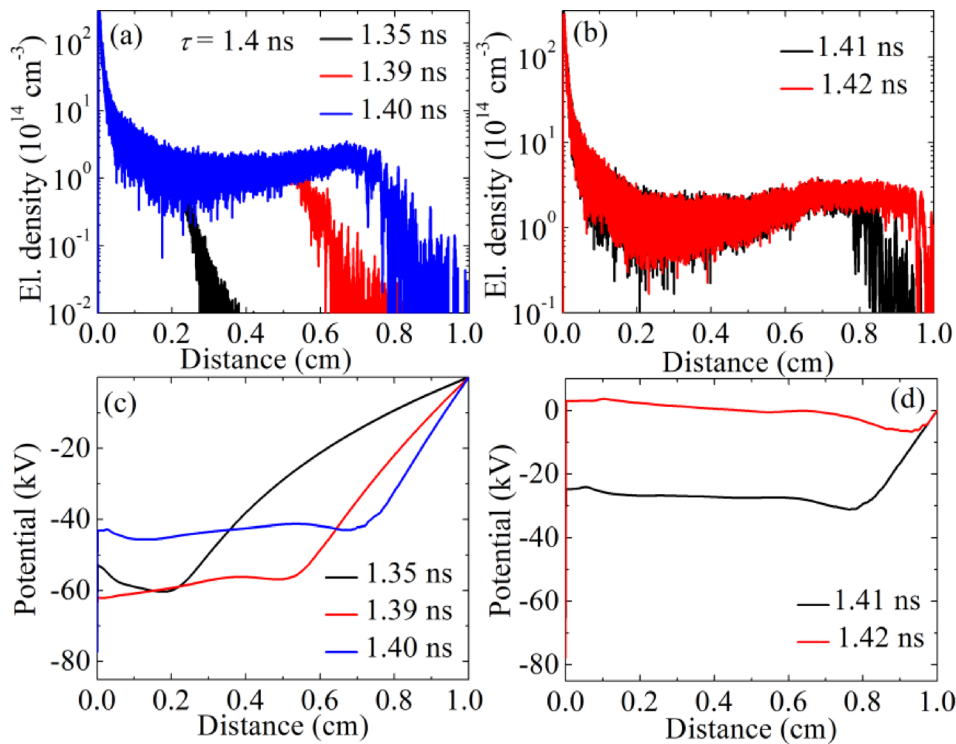


FIG. 8. [(a) and (b)] Electron density and [(c) and (d)] potential distributions obtained at different times; H_2 gas pressure is 2×10^5 Pa, and field emission is switched off at $\tau = 1.4$ ns.

rather dense ($\sim 10^{12} \text{ cm}^{-3}$) seeding plasma electrons. Then, the discharge develops in the form of a streamer propagating through this background plasma with the velocity of $\sim 10^8$ m/s. This allows runaway electrons to acquire more energy than $e|U_C|$ due to acceleration by the electric field at the head of the streamer. The number of these anomalous energetic electrons does not exceed 0.1% of the total number of FE electrons. The peak plasma density of $\sim 10^{17} \text{ cm}^{-3}$ was obtained in the vicinity of the cathode, while the electric field in the plasma channel was $\sim 7 \times 10^6$ V/m.

Finally, the influence of the FE switch-off time was analyzed. It was obtained that an early switch-off stops the ionization wave propagation. The bridging of the cathode-anode gap was realized by means of the RAEs remained in the gap. However, a late FE switch-off does not stop the ionization wave propagation. This was explained by the injection of the large number of electrons from the cathode prior to the FE switch-off. As a consequence, a large number of RAEs were

present in the cathode-anode gap, which drives the ionization wave propagation.

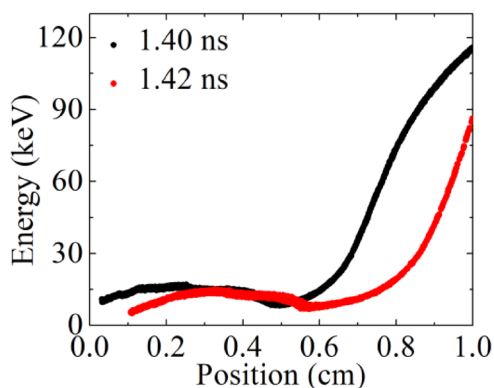


FIG. 9. Phase space of field emission (FE) electrons obtained at two different times; H_2 gas pressure is 2×10^5 Pa, and FE is switched off at $\tau = 1.4$ ns.

- ¹L. P. Babich, T. V. Loiko, and V. A. Tsukerman, *Phys.-Usp.* **33**, 521 (1990).
- ²V. F. Tarasenko and S. I. Yakovlenko, *Phys.-Usp.* **47**, 887 (2004).
- ³L. P. Babich, *High-Energy Phenomena in Electric Discharges* (Futurepast, Arlington, Virginia, 2003), Vol. 2.
- ⁴*Runaway Electrons Preionized Diffuse Discharges*, editor by V. F. Tarasenko (Nova Publishers, New York, 2015).
- ⁵Yu. D. Korolev and G. A. Mesyats, *The Physics of Pulse Breakdown* (Nauka, Moscow, 1991) (in Russian).
- ⁶G. A. Mesyats, M. I. Yalandin, K. A. Sharypov, V. G. Shpak, and S. A. Shunailov, *IEEE Trans. Plasma Sci.* **36**, 2497 (2008).
- ⁷V. F. Tarasenko, E. Kh. Baksht, A. G. Burachenko, I. D. Kostyrya, M. I. Lomaev, and D. V. Rybka, *IEEE Trans. Plasma Sci.* **38**, 741 (2010).
- ⁸G. A. Mesyats and M. I. Yalandin, *IEEE Trans. Plasma Sci.* **37**, 785 (2009).
- ⁹S. Ya. Belomytsev, I. V. Romanchenko, V. V. Ryzhov, and V. A. Shklyayev, *Tech. Phys. Lett.* **34**, 367 (2008).
- ¹⁰V. A. Shklyayev and V. V. Ryzhov, *Tech. Phys. Lett.* **37**, 72 (2011).
- ¹¹S. N. Ivanov, V. V. Lisenkov, and V. G. Shpak, *J. Phys. D: Appl. Phys.* **43**, 315204 (2010).
- ¹²T. Shao, V. F. Tarasenko, Ch. Zhang, E. Kh. Baksht, D. Zhang, M. V. Erofeev, Ch. Ren, Y. V. Shutko, and P. Yan, *J. Appl. Phys.* **113**, 093301 (2013).
- ¹³T. Shao, V. F. Tarasenko, Ch. Zhang, D. S. Beloplotov, W. Yang, M. I. Lomaev, Z. Zhou, D. A. Sorokin, and P. Yan, *Phys. Lett. A* **378**, 1828 (2014).
- ¹⁴S. Yatom and Y. E. Krasik, *J. Phys. D: Appl. Phys.* **47**, 215202 (2014).
- ¹⁵S. Yatom, V. Vekselman, J. Z. Gleizer, and Ya. E. Krasik, *J. Appl. Phys.* **109**, 073312 (2011).
- ¹⁶S. Yatom, S. Tskhai, and Ya. E. Krasik, *Phys. Rev. Lett.* **111**, 255001 (2013).
- ¹⁷D. Levko, S. Yatom, V. Vekselman, J. Z. Gleizer, V. Tz. Gurovich, and Ya. E. Krasik, *J. Appl. Phys.* **111**, 013303 (2012).
- ¹⁸D. Levko and L. L. Raja, *J. Appl. Phys.* **119**, 153301 (2016).
- ¹⁹N. Yu. Babaeva and G. V. Naidis, *Phys. Plasmas* **23**, 083527 (2016).
- ²⁰E. Marode, Ph. Dessante, and P. Tardiveau, *Plasma Source Sci. Technol.* **25**, 064004 (2016).
- ²¹N. Yu. Babaeva, Ch. Zhang, J. Qiu, X. Hou, V. F. Tarasenko, and T. Shao, *Plasma Source Sci. Technol.* **26**, 085008 (2017).

- ²²V. F. Tarasenko, E. K. Baksht, D. V. Beloplotov, A. G. Burachenko, I. D. Kostyrya, M. I. Lomaev, D. V. Rybka, and D. A. Sorokin, *JETP Lett.* **102**, 350 (2015).
- ²³A. M. Boichenko, *Tech. Phys.* **56**, 317 (2011).
- ²⁴L. P. Babich and T. V. Loiko, *JETP Lett.* **101**, 735 (2015).
- ²⁵G. A. Askaryan, *JETP Lett.* **2**, 113 (1965); available on-line http://www.jetpleters.ac.ru/ps/1598/article_24493.shtml.
- ²⁶J. Qin and V. P. Pasko, *J. Phys. D: Appl. Phys.* **47**, 435202 (2014).
- ²⁷C. Li, J. Teunissen, M. Nool, W. Hundsdorfer, and U. Ebert, *Plasma Source Sci. Technol.* **21**, 055019 (2012).
- ²⁸D. V. Rose, D. R. Welch, R. E. Clark, C. Thoma, W. R. Zimmerman, N. Bruner, P. K. Rambo, and B. W. Atherton, *Phys. Plasmas* **18**, 093501 (2011).
- ²⁹See <https://physics.nist.gov/cgi-bin/Ionization/table.pl?ionization=H2> for Electron-H₂ ionization cross section.
- ³⁰See www.lxcat.net/Biagi for Biagi database.
- ³¹Yu. P. Raizer, *Gas Discharge Physics* (Springer-Verlag, Berlin, 1991).
- ³²I. K. Kikoin, *Tables of Physical Quantities* (Atomizdat, Moscow, 1976) (in Russian).
- ³³C. Zhang, V. F. Tarasenko, T. Shao, E. Kh. Baksht, A. G. Burachenko, P. Yan, and I. D. Kostyrya, *Laser Part. Beams* **31**, 353 (2013).
- ³⁴E. Kh. Baksht, A. G. Burachenko, and V. F. Tarasenko, *Tech. Phys.* **60**, 1645 (2015).
- ³⁵C. H. Shon, H. J. Lee, and J. K. Lee, *Comput. Phys. Commun.* **141**, 322 (2001).
- ³⁶S. I. Yakovlenko, *Tech. Phys.* **49**, 1150 (2004).